On modelling conjugated heat transfer in the thin slab CC mold and solid shell formation under the applied EMBr

To cite this article: A Vakhrushev *et al* 2023 *IOP Conf. Ser.: Mater. Sci. Eng.* **1274** 012023

IOP Conf. Series: Materials Science and Engineering 1274 (2023) 012023 doi:10.1088/1757-899X/1274/1/012023

On modelling conjugated heat transfer in the thin slab CC mold and solid shell formation under the applied EMBr

A Vakhrushev[1], E Karimi-Sibaki[1], M Wu[2], A Ludwig[2], G Nitzl[3], Y Tang[4], G Hackl[4], J Watzinger[5], J Bohacek[6], A Kharicha[1],

[1]Christian-Doppler Lab for Metallurgical Applications of Magnetohydrodynamics, University of Leoben, Franz-Josef-Str. 18, 8700 Leoben, Austria
[2]Chair of Simulation and Modeling of Metallurgical Processes, University of Leoben, Franz-Josef-Str. 18, 8700 Leoben, Austria
[3]RHI Magnesita GmbH, Kranichberggasse 6, 1120, Vienna, Austria
[4]RHI Magnesita GmbH, Technolgy Centre, Magnesitstrasse 2, 8700, Leoben, Austria
[5]Primetals Technologies, Turmstrasse 44, 4031, Linz, Austria
[6]Heat Transfer and Fluid Flow Laboratory, Faculty of Mechanical Engineering, Brno University of Technology, 61669 Brno, Czech Republic

E-mail: abdellah.kharicha@unileoben.ac.at

Abstract. Continuous casting (CC) became one of the dominant steel production technologies throughout last decades. Better quality, energy savings and high production rates are the main aims of the research especially in the field of the thin slab casting (TSC). The electromagnetic brake (EMBr) is applied to control the highly turbulent flow after the fresh melt is fed through the ports of a submerged entry nozzle (SEN). The numerical modelling is a perfect tool to investigate the multiphase phenomena of the turbulent flow in the CC mold, heat transfer and solidification coupled with the effects of the magnetohydrodynamics (MHD). Traditionally the heat transfer in the CC mold during the numerical simulations is predefined by the heat flux profile which could be taken from the plant measurements, published data, or is described by the semi-empirical formulas. In all these cases the heat extraction in the CC mold cavity is strictly predefined and is not significantly influenced by the transient flow behavior. Moreover, the heat flux, used in a simulation, is frequently measured for the different flow pattern inside the mold. That is especially important when the EMBr effects on the solid shell formation are investigated. Thereby, the presented study considers the coupled heat transfer in the water-cooled copper mold, including the averaged thermal resistance between the slab and mold, implemented using OpenFOAM® open-source CFD software. The melt flow, the temperature field, and the induced electric current density are compared between the traditional approach (the applied heat flux) and the modelled heat transfer in the TSC mold. Different scenarios are studied without and with the applied magnetic field.

1. Introduction

During a thin slab casting (TSC) due to the narrow profile of the continuous casting (CC) mold a strong turbulence is generated after the fresh melt is fed through the ports of the submerged entry nozzle (SEN). As it was shown previously, the turbulent flow has a strong influence on the

solidification by interaction with the mushy zone [1–3]. Due to the partial remelting of the solid shell the risks of a breakout dramatically grow [4–6]. The application of the magnetic field in the form of the electromagnetic braking (EMBr) became an efficient flow control technology through last decades [7]. A very recent study has enlightened that the complex topology of the Lorenz force is not limited (as expected) to the damping effects only, but results in the entrainment of the quiescent melt into the motion and results in the formation of the reverse flow zones [8–10].
The melt flow and the distribution of the superheat in the TSC process are significantly altered under the EMBr action. Thereby an accurate model of the heat transfer in the CC mold is desired to predict those changes. Typically, such models consider the melt/shell, skin/shell and mold/skin contact and formation of the solid and liquid layers of the slag film as well as the air gap growth [11]. However, they become computationally demanding and, to overcome such a bottle neck, are reduced to the 2D-slice or even 1D models where the turbulent melt flow is over-simplified.
In the presented study, a single mesh approach is applied to simulate the turbulent flow together with the solidification, thermal resistance of a slag skin and the air gap, and with the heat transfer in the water cooled copper mold [12]. The electric potential method was used to tackle the magnetohydrodynamics effects [13]. The proposed method appeared to be robust and showed a good agreement with the corresponding experimental measurements [1,14].

2. Numerical model

2.1. Mold heat transfer model

Figure 1 display the simulation domain. A thin gap region was introduced between the melt bulk and the mold. The numerical mesh was significantly refined to resolve the gap. The geometry of the simulated mold corresponds to the effective thickness of the copper plates along the wide face (25 mm) and at the narrow side (18 mm) published elsewhere [14]. The cooling water temperature was assumed to be uniform (323.15 K) and will be adjusted in the future studies according to the recent publications [15]. The casting speed of 5.5 m/min was used in the simulation.
Traditionally, to model the solidification during CC process, a heat flux along the casting direction at the mold side of the solid shell is defined as boundary condition. It is commonly taken from literature for the similar mold designs, estimated from the on-site temperature measurements, defined by the semi-empirical formulas or modeled directly [1,14–16]. Accordingly, the temperature normal gradient is determined at the shell surface from the imposed heat flux distribution $Q(z)$ as following:

$$-\lambda \cdot \nabla_{\mathbf{n}} T = -Q(z), \tag{1}$$

where z is the distance from the meniscus, λ corresponds to the thermal conductivity and $\mathbf{n}$ is the wall normal vector oriented inward. It should be emphasized that the boundary condition (1) defines a fixed rate of the extracted heat. In such conditions, the model cannot respond accurately to the strong and fast changes in the temperature field caused by an EMBr or due to a SEN flow asymmetry [3].
In the presented study an alternative to the Neumann-type boundary condition (1) was chosen. As schematically shown in figure 2(a), it includes the heat transfer across TSC mold plates considering a thermal resistance between the shell surface and the mold hot face. The Robin-type boundary condition at the copper mold / cooling water interface is applied in the form:

$$-\lambda_{\text{mold}} \nabla_{\mathbf{n}} T|_{\text{mold}-\text{water}} = -\text{HTC}(z) \cdot (T_{\text{cold}} - T_{\text{water}}), \tag{2}$$

where $\text{HTC}(z)$ corresponds to the heat transfer coefficient between the mold cold face and the cooling water. The condition (2) and the complex heat transfer inside the mold plates and along the gap region give more degrees of freedom in comparison to the expression (1). Since the heat transfer coefficient is not provided, the procedure described below is applied to estimate the $\text{HTC}(z)$ distribution.
Figure 2(b) displays the mold heat flux (blue dashed line) along the casting direction z. Based on the solidification modelling using the traditional approach a time-average slab surface temperature T_{shell} was obtained, red line in figure 2(b). The temperature curve slightly recovers towards the mold's exit,

IOP Conf. Series: Materials Science and Engineering 1274 (2023) 012023 doi:10.1088/1757-899X/1274/1/012023

which is typically observed by thermocouples measurement for the continuous casting [11,17]. The HTC is estimated based on the applied heat flux Q and predicted slab surface temperatures T. The effective gap resistance R_{gap} is introduced representing the slag skin layer and formed air gap; it linearly increases from the meniscus level down to the mold exit. The slag rim is not considered.

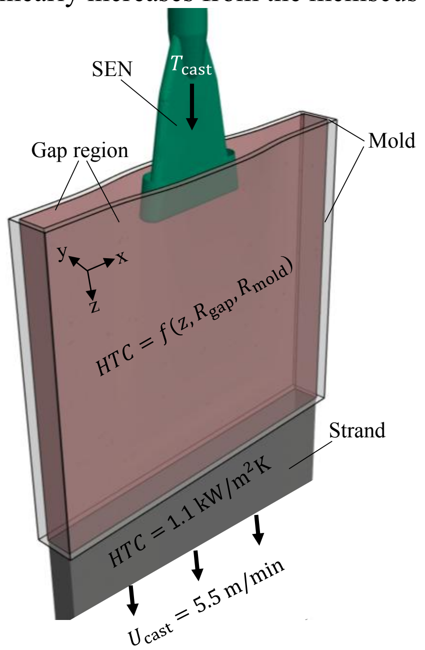

Figure 1. Simulation domain including SEN, TSC mold, gap region, strand part and corresponding boundary conditions.

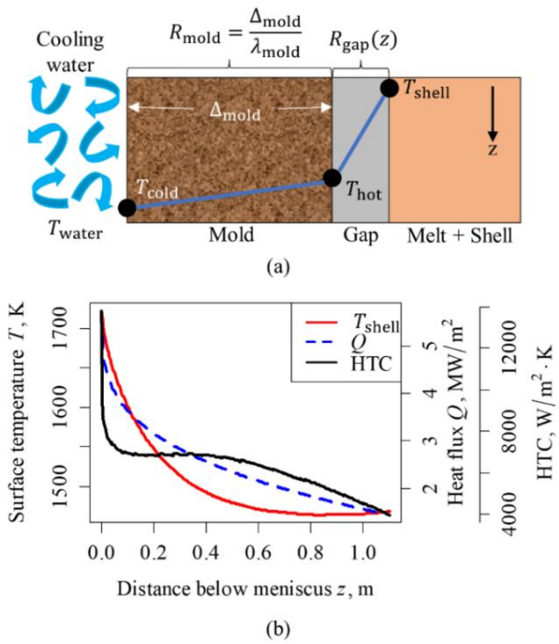

Figure 2. Heat transfer model: (a) shell-to-mold region; (b) imposed heat flux Q, modelled shell surface temperature T_{shell}, and estimated HTC(z).

By adding the mold thermal resistance R_{mold}, see figure 2(a), the HTC is obtained from:

$$\text{HTC}(z) = \Big((T_{\text{shell}} - T_{\text{water}})/Q(z) - \big(R_{\text{gap}} + R_{\text{mold}}\big) \Big)^{-1}, \tag{3}$$

where the reference temperature of coolant T_{water} is 323.15 K. The only unknown in equation (3) is the effective resistance R_{gap}. Assuming its linear variation along the casting direction, it was adjusted to fit the experimental measurements of the mold's cold face temperatures and the modelled predictions of the liquid slag layer [11,18]. The calculated distribution of HTC(z), shown in figure 2(b) with a black line, was used in further modelling. The cooling of the strand is described by an effective HTC of 1100 W/m^{2}K, obtained from the experimental measurements by solving the inverse conduction problem [19].

2.2. *Turbulent flow with solidification and MHD effects*

The momentum equation was used in the mixture volume average approach as

$$\rho \left[\frac{\partial \vec{u}}{\partial t} + \nabla \bullet (\vec{u} \otimes \vec{u}) \right] = \nabla \bullet [\text{dev}(\boldsymbol{\sigma}_{\text{tot}}) - p\mathbf{I}] + \vec{F}_{\text{mush}} + \vec{F}_{\text{MHD}} + \vec{F}_{\text{damp}}, \tag{4}$$

where the total stress $\boldsymbol{\sigma}_{\text{tot}}$ incorporate molecular viscous forces and the turbulence contribution by Reynolds stress modelling using large eddy WALE sub-grid scale model [20]. The Darcy force $\vec{F}_{\text{mush}}$ represents the drag between the mushy zone and the liquid melt [1]. The Lorentz force $\vec{F}_{\text{MHD}}$ acting due to the applied magnetic field is calculated using the electric potential method [13]. The details of the MHD model implementation considering the shell conductivity can be found elsewhere [8,9]. The damping source $\vec{F}_{\text{damp}}$ refers to a single mesh approach restricting motion to the melt region only [12].

The energy equation considering solidification is derived with respect to temperature T [3]:

$$\rho C_{\mathrm{p}}\left[\frac{\partial T}{\partial t}+\nabla\bullet(\vec{u}T)\right]=\nabla\bullet\lambda\nabla T+\rho L\left[\frac{\partial f_{\mathrm{s}}}{\partial t}+\nabla\bullet(f_{\mathrm{s}}\cdot\vec{u}_{\mathrm{s}})\right],\tag{5}$$

with the specific heat C_{p}, latent heat of fusion L, and liquid and solid fractions satisfying $f_\ell + f_{\mathrm{s}} = 1$. The important details of an implementation, considering the TSC funnel curvature, distribution of the solid velocities $\vec{u}_{\mathrm{s}}$ and the effects of the latent heat advection were published earlier [1,2,21,22]. All models were developed as an in-house code using OpenFOAM® finite volume libraries [23].

3. Simulation results

Next, the described heat extraction model was used to simulate the solidification during the TSC process without and with the magnetic field of the electromagnetic brake. The schematics of the applied EMBr is shown in figure 3(a). The modeled induced electric current lines are detailed in figure 3(b) indicating the insulating slag skin layer preventing the e-current going through the highly conductive copper mold. Simultaneously, the closure of the e-current lines through the solid shell is observed. The predicted hot and cold face temperatures of the TSC mold are resented in figure 3(c).

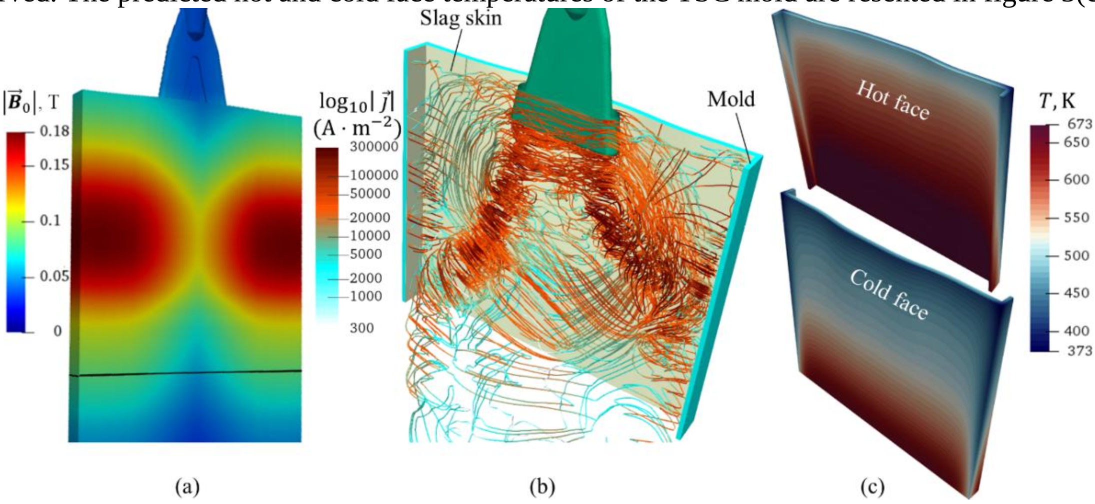

Figure 3. Modelling of the EMBr during a thin slab casting: (a) applied magnetic field; (b) induced electric current lines; (c) temperature distribution along the hot and cold faces of the TSC mold.

The comparison between the applied heat flux model and the proposed approach including the heat transfer in the mold is detailed in figure 4. For the case without applied magnetic field, the velocity fields in figures 4(a) and 4(c) are very similar, and no obvious difference was detected. However, for the temperature field in figures 4(b) and 4(c) the old model predicted slightly colder melt in the center. The application of the electromagnetic braking stabilizes the flow forming symmetric upper rolls and uniform flow closer to the molds exit, as observed from figure 5. More superheat is kept at the upper part of the mold at the meniscus level, which is highly desired in the CC process due to higher flux melting rate, uniform solidification, reduction of a frozen meniscus risk, etc.

The MHD flow including solidification is compared for two models in figure 5. With the EMBr the new model showed faster melt flow in the upper rolls by comparing figures 5(a) and 5(d). Again, colder central part was detected near molds exit for the old model, figure 5(b). Slightly more induced electric current is presented at the top part of the mold for the case of the new model in figure 5(f).

Thus, it can be seen, that with the dramatically changing flow pattern the difference between two models grows. Next study is to verify and detail of this difference using experimental data.

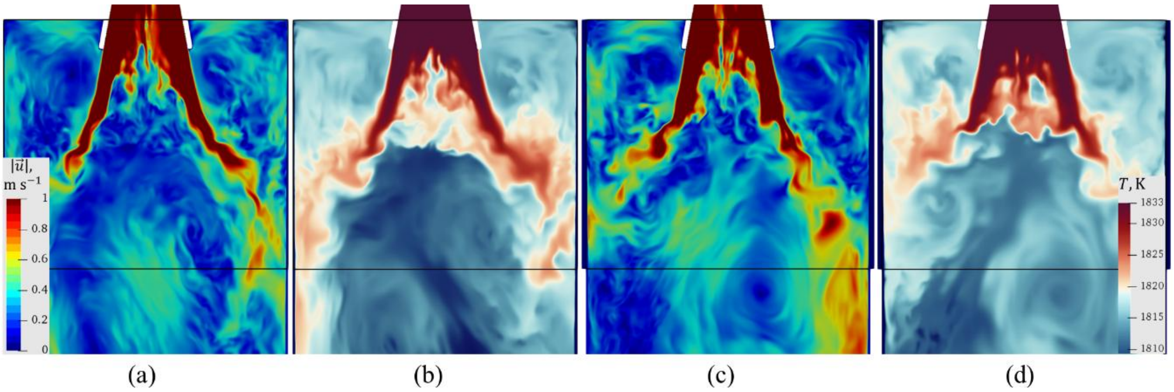

Figure 4. Simulation results for the flow velocity $\vec{u}$ and the temperature field T for the cases without EMBr: (a)-(b) imposed heat flux model; (c)-(d) model with the heat transfer across the mold.

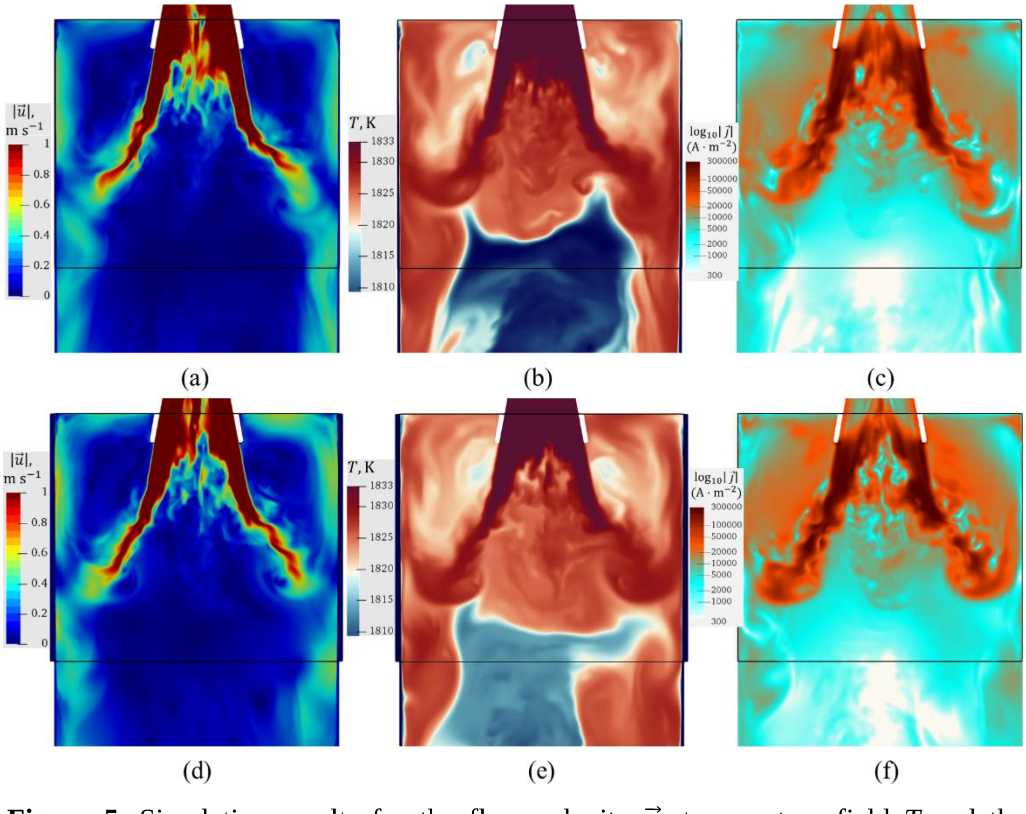

Figure 5. Simulation results for the flow velocity $\vec{u}$, temperature field T and the induced electric current $\vec{j}$ considering applied EMBr of 180 mT: (a)-(c) imposed heat flux model; (d)-(f) model with the heat transfer across the mold.

4. Conclusions

In the presented study a heat extraction model was introduced including a thermal resistance between the shell and the TSC mold hot wall. The simplified water cooling of the mold's cold face was modelled by estimating the heat transfer coefficient distribution along the casting direction. The magnetohydrodynamics forces were introduced to reflect the applied electromagnetic braking during TSC process. The simulated electrically insulating slag skin layer kept the induced e-current inside the liquid melt bulk, and the closure of the e-current lines through the solid shell was observed. The model showed good computational performance due to the employed single mesh approach. The obtained simulation results agreed with the old model. However, under drastically changing flow conditions, for example with the applied EMBr, the difference between two approaches grows. In the future study the model will be verified in detail using experimental data. The method will be extended by introducing the shell to skin and skin to mold contact models and considering temperature dependent properties.

5. Acknowledgments

The authors acknowledge the financial support by the Austrian Federal Ministry of Economy, Family and Youth and the National Foundation for Research, Technology and Development within the framework of the Christian Doppler Laboratory for Metallurgical Applications of Magnetohydrodynamics.

References

[1] Vakhrushev A, Wu M, Ludwig A, Tang Y, Hackl G and Nitzl G 2014 *Metall. Mater. Trans. B* **45** 1024–37
[2] Wu M, Vakhrushev A, Ludwig A and Kharicha A 2016 *IOP Conf. Ser.: Mater. Sci. Eng.* **117** 012045
[3] Vakhrushev A, Kharicha A, Karimi-Sibaki E, Wu M, Ludwig A, Nitzl G, Tang Y, Hackl G and Watzinger J 2022 *steel research int.* srin.202200088
[4] Iwasaki J and Thomas B G 2012 *Supplemental Proceedings* ed Tms (Hoboken, NJ, USA: John Wiley & Sons, Inc.) pp 355–62
[5] Luk'yanov S I, Suspitsyn E S, Krasilnikov S S and Shvidchenko D V 2015 *Int J Adv Manuf Technol* **79** 1861–8
[6] Zappulla M L S, Cho S and Thomas B G 2019 *Steel Res. Int.* **90** 1800540
[7] Thomas B G and Cho S M 2018 *IOP Conf. Ser.: Mater. Sci. Eng.* **424** 012027
[8] Vakhrushev A, Kharicha A, Liu Z, Wu M, Ludwig A, Nitzl G, Tang Y, Hackl G and Watzinger J 2020 *Metall. Mater. Trans. B* **51** 2811–28
[9] Vakhrushev A, Kharicha A, Karimi-Sibaki E, Wu M, Ludwig A, Nitzl G, Tang Y, Hackl G, Watzinger J and Eckert S 2021 *Metall. Mater. Trans. B* **52** 3193–207
[10] Kharicha A, Vakhrushev A, Karimi-Sibaki E, Wu M and Ludwig A 2021 *Phys. Rev. Fluids* **6** 123701
[11] Meng Y and Thomas B G 2003 *Metall. Mater. Trans. B* **34** 685–705
[12] Vakhrushev A, Kharicha A, Wu M, Ludwig A, Tang Y, Hackl G, Nitzl G, Watzinger J and Bohacek J 2021 *Metals* **11** 1375
[13] Davidson P A 2001 *An Introduction to Magnetohydrodynamics* (Cambridge University Press)
[14] Camporredondo S. J E, Castillejos E. A H, Acosta G. F A, Gutiérrez M. E P and Herrera G. M A 2004 *Metall. Mater. Trans. B* **35** 541–60
[15] Niu Z, Cai Z and Zhu M 2020 *Ironmaking & Steelmaking* **47** 1135–47
[16] Zhang H and Wang W 2017 *Metall. Mater. Trans. B* **48** 779–93
[17] Santillana B, Hibbeler L C, Thomas B G, Hamoen A, Kamperman A and Knoop W V D 2008 *ISIJ Int.* **48** 1380–8
[18] Meng Y and Thomas B G 2003 *Metall and Materi Trans B* **34** 707–25
[19] Bohacek J, Kominek J, Vakhrushev A, Karimi-Sibaki E and Lee T-W 2021 *OpenFOAM Journal* **1** 27–46
[20] Nicoud F and Ducros F 1999 *Flow, Turbulence and Combustion* **62** 183–200
[21] Vakhrushev A, Kharicha A, Wu M, Ludwig A, Nitzl G, Tang Y, Hackl G, Watziger J and Rodrigues C M G 2019 *IOP Conf. Ser.: Mater. Sci. Eng.* **529** 012081
[22] Vakhrushev A, Kharicha A, Wu M, Ludwig A, Nitzl G, Tang Y, Hackl G, Watzinger J and Rodrigues C M G 2022 *J. Iron Steel Res. Int.* **29** 88–102
[23] Weller H G, Tabor G, Jasak H and Fureby C 1998 *Comput. Phys.* **12** 620